Investigating the Energetics of Fluid-rock Interactions in Shale Nanopore using Molecular Dynamics Simulation

Zelong Zhang,*[,†] Haoran Liu, [‡,⊥] and Jianwei Wang[†,§]

[†]Department of Geology and Geophysics, Louisiana State University, Baton Rouge, LA 70803, United States

[‡]Department of Experimental Statistics, Louisiana State University, Baton Rouge, LA 70803, United States

[⊥]Department of Oceanography and Coastal Sciences, Louisiana State University, Baton Rouge, LA 70803, United States

[§]Center for Computation and Technology, Louisiana State University, Baton Rouge, LA 70803, United States

Corresponding to: zelongz@lsu.edu

Abstract

Understanding the fluid-rock interactions in shale nanopores is essential for the characterization of the transport and storage of hydrocarbon in oil reservoir rocks of tight formations such as shale. Due to strong surface effect in nanospace and the heterogeneous nature of hydrocarbon systems, it is a great challenge to conduct experiments in shale nanopore. Molecular Dynamics simulations were applied to investigate the interaction of light oils with calcite and kerogen surfaces. Octane and octanthiol molecules were used to represent non-polar and polar oil compounds. A kerogen model was implemented to build the organic surfaces of type II kerogen which is the major constituent of shale organics. Calcite {104} surface was used to represent the shale mineral due to its hydrophilic property of its surfaces and its ubiquitous presence in formation rocks, especially in carbonate shales. Umbrella Sampling method together with Weighted Histogram Analysis Method was employed to calculate the Gibbs free energy surface of desorption of oil molecules on the surfaces of kerogen and calcite. Because the desorption process in this study is reversible and is the reserved process of adsorption. The amount of energy required for desorption is the same for adsorption. The effects of oil polarity, size of oil molecular cluster, and water on the free energy were investigated. The results show that at molecular scale, the free energy of desorption of oil molecules is significantly reduced from both kerogen and calcite surfaces if water is presented. For polar oil molecule, the free energy of desorption is higher than that of non-polar oil at both calcite and kerogen surfaces. The organic kerogen surface exhibits stronger binding energies of oil molecules than the inorganic calcite. These findings suggest that 1) polar oil compounds require more effort to be recovered than non-polar ones, 2) oil clusters of a smaller size are harder to be displaced than a larger size, and 3) the presence of water decreases the free energy of desorption. This study provides energetic perspective of the interactions and insights on the oil recovery in shale formations. The methodology presented in this study demonstrates that MD simulation is capable to 1) evaluate the impact of different factors to the oil recovery in shale play and 2) offer valuable implications for developing novel technologies of oil recovery from unconventional shale.

43 **TOC**

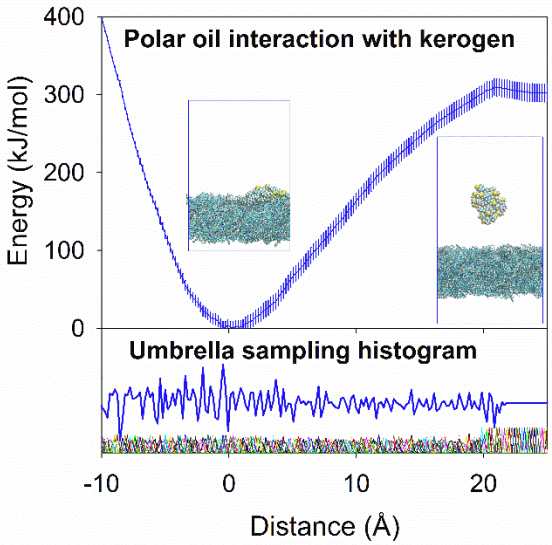
Polar oil interaction with kerogen
Umbrella sampling histogram
Energy (kJ/mol)
400
300
200
100
0
-10
0
10
20
Distance (Å)

44

1 Introduction

Ultra-tight formations, such as shale, bear abundant hydrocarbon fluid in poorly connected nanoscale pores with extremely low porosity and permeability.[1,2] The flow properties of transport and storage of fluid confined in nanopores deviates substantially from those of its bulk phase. This deviation is largely caused by the surface interactions within nanospace.[3–5] The interactions between the fluid and pore surface can affect a large portion of confined fluid molecules depending on the pore size and interfacial interactions, which leads to dramatic differences in the behaviors of fluid migration and storage in nanopores, compared to those of bulk phase fluid.[6,7] Significant amounts of hydrocarbon in ultra-tight reservoirs are confined in the nanopores,[8] mostly in organics and associated with minerals.[9,10] To understand how the hydrocarbon is stored in the formation rocks, it is vitally important to investigate the interfacial interactions between the hydrocarbon fluid and nanopore surfaces in ultra-tight formation. Since oil recovery process is linked to the interfacial interactions between oil molecules and nanopore surfaces, characterizing the free energy changes involved in the interfacial interactions is essential to understand and to predict the transport and storage behavior of oil in shale.[11] The free energy behavior can determine the favorable thermodynamic conditions to promote oil recovery. This approach can lead to important implications for oil recovery efforts.

To probe the interfacial interactions at nanoscales requires atomistic- and molecular-level characterization. Both experimental and computational approaches have been applied to study the hydrocarbon fluid behavior in shale at nanoscale. Extensive experimental studies have been conducted on the shale formation to characterize the organic content[12,13], pore structure[9,14–16], and petrophysics[9,17–19]. These studies aimed to calibrate the empirical models in reservoir engineering

to describe the fluid flow[20,21] and to provide implications for reservoir assessment and production optimization.[10] However, it is challenging to interpret the dynamics and kinetics of interface interactions without knowing the molecular scale details given the compositional and structural heterogeneity of shale formations. Understanding of the shale systems heavily relies on the characterization technologies to conduct experiments on surfaces and interfaces[22–24] such as Focus Ion Beam Scanning Electron Microscopy (FIB-SEM),[19,25,26] Transmission Electron Microscopy (TEM),[26,27] Atomic Force Microscopy (AFM),[1,20,28] X-ray Diffraction (XRD),[29,30] X-ray microtomography (Micro-CT),[31,32] Nuclear Magnetic Resonance (NMR),[33,34] etc. Implementing these methodologies become challenging at molecular level and even infeasible at atomic scale in order to characterize microscopic phenomena. Unlike experiments, computational simulations can study physical phenomena over a wide range of scale across space and time,[35] directly connecting the microscopic details of a system with macroscopic properties of experimental interest.[36] Simulations based on quantum mechanics (QM) can describe phenomena of subatomic resolution. However, due to the intensive computation of QM simulation, the size, time, and complexity of studies systems are significantly limited.[35–37] Molecular and atomistic simulations, built on classical molecular mechanics (MM), such as Monte Carlo (MC) simulation and Molecular Dynamics (MD) simulation, are more appropriate than QM methods to address the issues of size and complexity of hydrocarbon systems. MC methods are stochastic approach, suitable for analyzing system equilibrium, while MD techniques are deterministic, favorable to study both equilibrium and transport properties of a given system.[36,37] Thus, this study used MD in order to reveal the kinetics of fluid-rock interactions of nanoscale. Currently, there are several studies using MD to investigate oil-rock interactions: 1) the adsorption and diffusion properties of hydrocarbon fluid in shale organic

phase, type II kerogen;[38–42] 2) the permeation of hydrocarbon fluids through kerogen-like nanoporous carbon;[7,43] 3) slippage and displacement of hydrocarbon flow in quartz and calcite slits;[44–46] 4) detachment of oil cluster from silicate surfaces in solution;[47] 5) adsorption of methane in carbon slit-pores;[48] and 6) adsorption of light oil molecules on montmorillonite slits[49]. These studies evaluated the effect of nanopores on the properties of hydrocarbon fluid, such as bulk viscosity, contact angle, and slippage. The energetic aspect of the hydrocarbon/shale interaction essentially remains intact and hence limited kinetic information is reported.

The present study demonstrates the feasibility of computational approach to evaluate the free energy profile of oil compounds desorption from shale surfaces. Calculation of free energy profile by Umbrella Sampling is widely used in computational biology and biochemistry.[50] To date, this technique has not been used to investigate the oil interactions with shale media especially organic kerogen or to provide kinetic information on the adsorption and desorption processes. We examine the surfaces of kerogen and calcite to evaluate the effect of four different variables including oil polarity (polar vs non-polar oil), oil cluster size (single molecule oil vs 30-molecule oil cluster), surface composition (inorganic calcite mineral vs organic kerogen), and surface water (the presence vs the absence of surface water). Profiling the free energy of oil-rock interactions in nanopores provides a kinetic insight of hydrocarbon behaviors in unconventional shale reservoir, a multi-phased nano-porous system of rich organic content.

2 Method

2.1 Molecular models for oil, kerogen, and calcite

Typically, crude oil has more than 45% non-polar (e.g. alkanes and cycloalkanes) and less than 15% polar species (e.g. N-, S-, O- and metal-containing compounds).[51,52] Polar components can significantly affect properties of hydrocarbon fluid in reservoir such as viscosity, contact angle, interfacial activity, emulsion, and chemical stability.[2,53,54] The oil-rock interaction is largely attributed by the polar species,[55] particularly in shale since organic phases usually retain more polar components than minerals[2]. Molecular polarity can be described by the dipole moments of molecules. Thioalkanes are common sulfur compounds found in crude oils.[56] Shale oil has high content of light oil (C_1-C_9).[57,58] Therefore, we selected 1-octanethiol ($C_8H_{18}S$) with a dipole moment of 2.9 D[59] and its non-polar counterpart n-octane (C_8H_{18}) with no dipole moment. These two compounds were employed as models for polar and nonpolar oil in shale, as shown in Figure 1. In addition, we prepared two oil clusters consisted of 30 molecules of octanethiol and octane, respectively. Water used in the simulation is the SPC model with a dipole moment of 2.27 D, comparable to the experimental measurement 1.85 D.[60]

Shale's composition is highly complicated, which contains inorganic and organic constituents. Inorganic phases consist of three major minerals: clays, quartz, and carbonates (calcite and dolomite)[14]. We chose calcite {104} face as a hydrophilic mode of shale inorganic surface. The calcite {104} is a flat stoichiometric surface, which is one of most common mineral faces occurred in both geological and biological systems and has been well studied both computationally and experimentally.[61] The key organic phase in shale involved in the interaction with hydrocarbon is kerogen.[2,62,63] Despite the complexity of kerogen in reservoir formations[64], many studies used graphene to represent kerogen[7,43,48,65–68]. The vast differences between graphene and kerogen, such as bonding environment of functional groups[69,70] and surface morphology[64], give different chemical and mechanical properties[70,71]. Changing surface

properties can drastically alter the interfacial interactions with hydrocarbons, leading to different simulations results. To have a reasonable computation cost and to capture fundamental properties of kerogen, we employed a fragment molecule $C_{22}H_{13}ON$ derived from type II kerogen to build kerogen surfaces,[38] which is the most common kerogen in hydrocarbon-bearing shale formations[64]. The kerogen molecule has five benzene rings, a secondary amine, and a phenol group, resulting a polar compound. To create kerogen surfaces, the kerogen molecules were randomly added into a computational supercell of 18,944 atoms, periodic in x and y directions, and quenched from 3000 to 300 K (ramp) to stabilize and relax the surface.

The calcite {104} surface in Figure 2(b) was built with 1620 calcite molecules, six layers of calcite's {104} surface, with a dimension of approximately 7 × 7 × 2 nm with 8,100 atoms. The kerogen surface in Figure 2(a) was built with 511 kerogen molecules with a dimension of approximately 8 × 8 × 3 nm with 18,907 atoms as shown. Because of the ubiquitous presence in the reservoir formations, water molecules were added to interfaces of oil/surface interactions. To ensure the complete submergence of their interactions in water, 7,250 and 10,000 water molecules were added to the calcite surface of single oil molecule or oil cluster, respectively; while 7,500 and 10,000 water molecules were placed on kerogen surfaces of single oil molecule or oil cluster, respectively.

Previous experimental study indicates calcite {104} surface exhibits neutral charge due to the stoichiometry of Ca^{2+} and CO_3^{2-},[72,73] quartz and clay minerals have negative surface charge in the presence of surface water.[74,75] Kerogen surfaces can be negatively charged due to the deprotonation of functional groups, such as OH and NH. However, classical MD models only simulate non-bonded interactions, van der Waals interactions, and electrostatic interactions, whereas formation and breaking of covalent bonds are excluded unless specified by force field.

Both calcite and kerogen surfaces maintain electrical neutrality owing to the charge balance of each model molecule. Layers of alternating Ca^{2+} and CO_3^{2-} on calcite {104} created a polar surface, while the benzene rings and polar functional groups of kerogen molecule yielded polar and heterogenous surfaces of kerogen.

2.2 Molecular Dynamics (MD) Simulation and Gibbs Free Energy Profiles

MD simulations in this study were deployed using software package GROningen MAchine for Chemical Simulations (GROMACS). All simulations were under the three-dimensional periodic boundary condition. The OPLS-AA force field was used to describe oil molecules and kerogen.[76] The SPC potential is used to describe water molecule.[60] A previously developed force field was used for calcite.[77] All these potentials have been tested and are capable of producing satisfactory results on bulk and interfacial properties, which are consistent with experimental data.[78–80] For a typical umbrella simulation, 1 ns simulation was used for the system to reach equilibrium. Newton's equations of motion were integrated using the leap-frog scheme with a timestep of 1 fs; fast Smooth Particle-Mesh Ewald (SPME) electrostatics; Verlet cutoff-scheme; temperature coupling using a Nose-Hoover extended ensemble; and period of temperature fluctuations at equilibrium 0.1 ps. Simulations were visualized by Visual Molecular Dynamics (VMD) package.

Potential of mean force of the Gibbs free energy profiles for the oil interactions with different surfaces was computed by Umbrella Sampling and the Weighted Histogram Analysis Method (WHAM).[81,82] Gromacs package was used to carry out Umbrella Sampling simulations by running separate simulation windows along the reaction coordinate individually. In each

simulation window, a bias harmonic potential was applied to the system. With sufficient windows to overlap the entire reaction coordinate space, a free energy profile curve can be calculated by combining data from each window using WHAM. For each individual simulation window, the umbrella potential with a force constant 9000 $kJ \cdot mol^{-1} \cdot nm^{-2}$ was applied to maintain the distance between the oil and surface for 0.1 or 0.2 ns after using a constraint potential with a force constant 9000 $kJ \cdot mol^{-1} \cdot nm^{-1}$ for 0.1 ns to equilibrate the system. The simulation windows were generated by simulations pulling the oil into or away from the surfaces regardless of the presence of water.

The error analysis on energy profiles was performed by R. We used LOESS algorithm to fit the dataset of each energy profiles and bootstrap technique to calculate confidential interval of 95%. The computed errors listed as shown in Table 1 denoted by brackets. The fluctuations of free energy profile lines as shown in Figure S1 were consistent with the size of the error bar.

3 Results

Free energy surfaces in Figures 3-6 exemplify how the system energy changes as a function of the distance between oil compounds and surfaces. When the oils approach surface, energy required becomes large due to repulsive interactions. When the oils gradually move away from the surface, less energy is required until the minimal point which is the state of adsorption of the oil at the surfaces. The point that requires the least energy is the same state where oil molecule can freely be adsorbed on the surface. As the distance continuously increases, the energy increase until system reaches the energy plateau region where no additional energies are required to maintain distance between the oils and the surfaces.

202

203 ### 3.1 Oil interactions with kerogen

204 The free energy profiles in Figure 3 show the interaction energy changes as a function of
205 the distance between oil compounds and kerogen surfaces in the presence of water. Both the
206 minimal and plateau of free energy were observed; the desorption energies of these system are
207 17.0 ± 2.0 kJ/mol and 16.5 ± 3.3 kJ/mol for non-polar and polar single oil molecule and 371±
208 12.4 kJ/mol and 209 ± 7.0 kJ/mol for non-polar and polar oil clusters, respectively. In the
209 absence of water, oil molecules did not remain as a cluster at 300 K during the simulation long
210 enough for the umbrella sampling. To stabilize the oil cluster, a series of identical Umbrella
211 Sampling simulations were carried out under reduced system temperatures to extrapolate the
212 desorption energy at 300 K (detail was discussed in the SI). The desorption energies of oil cluster
213 on kerogen surfaces are 437 ± 13.5 kJ/mol for both polar and non-polar (Figure SI1). For the
214 single oil molecule, the desorption energies on kerogen in Figure 4 are 23.3 ± 3.5 kJ/mol and
215 39.5 ± 9.5 kJ/mol for non-polar and polar.

216

217 ### 3.2 Oil interactions with calcite

218 The energy profiles in Figure 5 shows how the free energy changes as a function of the
219 distance between oil compounds and calcite {104} surfaces in water. Unlike the rest free energy
220 profiles (described later), they exhibit a distinct pattern: as the distance increase, the free energy
221 quickly decreased to minimal and maintained at the same level to form a flatland. The minimal
222 value is the same as the suggested near zero energy for the desorption of the oil molecule. The

zero desorption energies indicate the attraction does not exist between the oil and the calcite surface in the presence of water.

For comparison, identical set of systems without water were simulated, of which the free energy profiles are depicted in Figure 6. The results show that 33.6 ± 3.9 kJ/mol and 18.0 ± 5.5 kJ/mol are required to desorb polar and non-polar oil molecules from calcite surfaces; 222 ± 36 kJ/mol and 198 ± 42 kJ/mol to desorb polar and non-polar oil clusters, respectively. According to the simulation output trajectory in the SI, the polar molecule was bound to the calcite surface through the functional group, which confirms a previous study on the adsorption of simple organic molecules on calcite {104}.[83] In addition, the thiol group –SH of polar oil appears to favor the sites of Ca^{2+} of calcite {104} surface, whereas the non-polar oil shows no preference of absorption sites.

4 Discussion

In this section, we will elaborate how on the desorption energies are affected by different system parameters, including shale surface composition, oil polarity, surface water, and oil clustering. The desorption energies of oil under these different conditions are compared in Table 1 together with their values normalized to kJ per molecule. We will also discuss the fundamental mechanisms that determine the interfacial interactions between oil and shale rock.

4.1 Effect of shale surface composition (kerogen/calcite)

Our study shows that the desorption energy of oil on calcite surfaces are systematically lower than on kerogen surfaces. We compared free energy profiles of calcite and kerogen surfaces with identical system parameters including oil polarity, oil cluster size, and surface water. When changing calcite into kerogen, the increment in desorption energy ranges from 5.3 to 17 kJ/mol for single-molecule oil and 210 to 372 kJ/mol for oil cluster. Regardless of molecular polarity, both single molecule oil and oil cluster requires higher desorption energy from kerogen than calcite, indicating oil recovery from organic phase of shale requires more efforts than calcite.

One major factor that contributes to the difference between kerogen and calcite is the surface morphology. Calcite {104} surface is well-structured, which has low surface area. Therefore, calcite has low sorption capacities.[84] The kerogen surface was created to be a porous and waxy structure in accordance with the experimental observation.[64,85] Therefore, the effective surface area on kerogen would be much higher than calcite, leading to a higher desorption energy for oil.

4.2 Effect of oil polarity

This study shows that molecular polarity plays imperative role during the oil desorption processes. For oil adsorbed on calcite surfaces, polar oil consistently requires higher desorption energies than its counterpart non-polar oil owing to the molecular dipole of both polar oil and calcite. However, the effect of polarity is complicated on kerogen surfaces. The desorption energies of the single molecule oil show that polar oil requires energy that is about two times of that of non-polar per molecule; whereas the desorption energies of polar and nonpolar oil are

approximately the same in the presence of water. For 30-molecule oil cluster, our calculation indicates that polar oil requires the same desorption energies as non-polar.

These phenomena can be explained by the dipole interactions. The polar oil creates dipole due to its uneven structure. Since there is no free ion in the systems, the intermolecular interactions are controlled by permanent dipole interactions, or Keesom interaction. As shown in SI Fig 4, the thiol functional group (–SH, yellow) of polar oil tend to be in proximity to the functional groups of kerogen molecules such as amine (–NH–, blue) and hydroxyl (–OH, red) upon contact at interfaces, which confirms the anticipated dipole interactions. Unlike polar oil, non-polar oil molecules have no dipole moment and therefore weaker desorption energies than polar oil. Thus, the affinity of polar oil with both calcite and kerogen surfaces is stronger than non-polar.[86] This postulation implies that the polar content of shale oil can significantly affect the oil/rock interactions in shale by changing the chemical environment at the interfaces.[53,87–89] High polar content in the oil fluid can bring additional challenge to oil recovery in tight formations of unconventional shale plays.

In addition, the similar energies for non-polar and polar oil clusters on kerogen suggest that the molecular polarity has insignificant impact on the interaction between 30-molecule cluster and kerogen surface. As shown in SI Fig 3, it is possible that the strong dipole interactions can promote the polar oil molecule to be in proximity by their functional groups, which can reduce the exposure of functional groups to the kerogen surfaces and therefore lead to a bonding that is mainly contributed by the interactions of non-polar part of polar molecule with kerogen surface. Therefore, the polar oil cluster behaves as the non-polar oil when they interact with kerogen surface. Another possible explanation is due the heterogenous nature of kerogen surface. The kerogen molecule is a large compound with five non-polar benzene rings and two

polar functional groups. Therefore, it is likely that affinity between non-polar groups of kerogen with non-polar oil is similarly strong as the polar groups of kerogen to polar oil.

Moreover, calcite {104} plane cannot be treated as non-polar surface, especially at nanoscale. Previous studies suggested that calcite {104} is overall non-polar because the alternating Ca^{2+} and CO_3^{2-} are closely packed and maintain charge balance.[90,91] Our study shows that at molecular level the calcite {104} is clearly favors the adsorption of the polar oil than non-polar oil due to the dipole moment possessed in each Ca^{2+} and CO_3^{2-} pair.

4.3 Effect of surface water

The presence of surface water reduces the oil desorption energy on all surface conditions, promoting the oil desorption for all the cases. As discussed previously, the molecules of water, calcite, and kerogen are all polar compounds with dipole moments; the surface water can easily be attracted to the surfaces of calcite and kerogen due to the dipole interaction, which reduces the surface area exposed to oil compound. Both water and polar oil have similarly potent dipole moments 2.9 D and 2.27 D, respectively. During the kinetic process of fluid/shale interactions, water was competing with oil compounds for surface adsorption, and consequently reducing the desorption energy. Interestingly, the effect of waters on calcite {104} surfaces was much more pronounced than on kerogen due to the hydrophilic nature of calcite. The affinity between calcite and water is stronger than calcite and oil, creating a strong oil-repellent surface of calcite in the presence of water.

4.4 Effect of oil clustering

Single molecule oil and 30-molecule oil cluster were tested in all simulation sets. Overall, the desorption energies required per molecule of oil cluster is substantially smaller than that of single molecule. This is mainly caused by different surface area per oil molecule exposed to the surface. Molecules in 30-molecule cluster has notably less surface area exposed compare to that of single molecule. Thus, the surface effect per molecule to oil cluster is less server than that to single molecule oil, which leads to the smaller desorption energies per molecule. Therefore, oil clusters of smaller size require higher desorption energies per molecule.

5 Summary

This study demonstrates Molecular Dynamics Simulation is capable to reveal the energetic details of oil/rock interactions at nanoscale. The changes on the system variables can be quantified by energetics. By varying system parameters such as surface composition, oil polarity, surface water, oil clustering, etc., the variations in desorption energy between different oil/rock interactions suggest that 1) the waxy and porous structure of kerogen has significant contribution to the increment of desorption energy owing to the large surface area and strong dipole moments of functional groups; 2) polar oil compounds require more effort to be recovered than non-polar. If the presence of polar content is substantial, it is necessary to treat shale oil as polar mixtures instead of non-polar for effective oil recovery; 3) dispersed oil compounds in nanopore tend to be more challenging to be recovered than clustered due to the effective surface area; 4) surface water facilitates the oil desorption by reducing the binding energy between oil and shale rocks. This study provides a fundamental approach to investigate the energy involved during oil/rock interactions at nanoscale, offering valuable implications for oil recovering from tight reservoirs especially in unconventional shale play.

Conflicts of interest

There are no conflicts to declare.

Acknowledgements

This research used resources of the National Energy Research Scientific Computing Center (NERSC), a U.S. Department of Energy Office of Science User Facility operated under Contract No. DE-AC02-05CH11231. Portions of this research were conducted with high performance computing resources provided by Louisiana State University (http://www.hpc.lsu.edu).

References

(1) Javadpour, F. Nanopores and Apparent Permeability of Gas Flow in Mudrocks (Shales and Siltstone). *J. Can. Pet. Technol.* **2009**, *48* (08), 16–21. https://doi.org/10.2118/09-08-16-DA.

(2) Jarvie, D. M. Shale Resource Systems for Oil and Gas: Part 2—Shale-Oil Resource Systems. **2012**, 89–119. https://doi.org/10.1306/13321447M973489.

(3) Sharma, P.; Ganti, S.; Bhate, N. Effect of Surfaces on the Size-Dependent Elastic State of Nano-Inhomogeneities. *Appl. Phys. Lett.* **2003**, *82* (4), 535–537. https://doi.org/10.1063/1.1539929.

(4) Auffan, M.; Rose, J.; Bottero, J.-Y.; Lowry, G. V.; Jolivet, J.-P.; Wiesner, M. R. Towards a Definition of Inorganic Nanoparticles from an Environmental, Health and Safety Perspective. *Nat. Nanotechnol.* **2009**, *4* (10), 634–641. https://doi.org/10.1038/nnano.2009.242.

(5) Boles, M. A.; Ling, D.; Hyeon, T.; Talapin, D. V. The Surface Science of Nanocrystals. *Nat. Mater.* **2016**, *15* (2), 141–153. https://doi.org/10.1038/nmat4526.

(6) Wang, Y. Nanogeochemistry: Nanostructures, Emergent Properties and Their Control on Geochemical Reactions and Mass Transfers. *Chem. Geol.* **2014**, *378–379*, 1–23. https://doi.org/10.1016/j.chemgeo.2014.04.007.

(7) Falk, K.; Coasne, B.; Pellenq, R.; Ulm, F.-J.; Bocquet, L. Subcontinuum Mass Transport of Condensed Hydrocarbons in Nanoporous Media. *Nat. Commun.* **2015**, *6*, 6949. https://doi.org/10.1038/ncomms7949.

(8) Javadpour, F.; Fisher, D.; Unsworth, M. Nanoscale Gas Flow in Shale Gas Sediments. *J. Can. Pet. Technol.* **2007**, *46* (10). https://doi.org/10.2118/07-10-06.

(9) Sondergeld, C. H.; Ambrose, R. J.; Rai, C. S.; Moncrieff, J. Micro-Structural Studies of Gas Shales; Society of Petroleum Engineers, 2010. https://doi.org/10.2118/131771-MS.

(10) Wang, F. P.; Reed, R. M. Pore Networks and Fluid Flow in Gas Shales; Society of Petroleum Engineers, 2009. https://doi.org/10.2118/124253-MS.

(11) Pohorille, A.; Chipot, C. Summary and Outlook. In *Free Energy Calculations: Theory and Applications in Chemistry and Biology*; Chipot, C., Pohorille, A., Eds.; Springer Series in CHEMICAL PHYSICS; Springer Berlin Heidelberg: Berlin, Heidelberg, 2007; pp 503–513. https://doi.org/10.1007/978-3-540-38448-9_14.

(12) Zhang, T.; Ellis, G. S.; Ruppel, S. C.; Milliken, K.; Yang, R. Effect of Organic-Matter Type and Thermal Maturity on Methane Adsorption in Shale-Gas Systems. *Org. Geochem.* **2012**, *47*, 120–131. https://doi.org/10.1016/j.orggeochem.2012.03.012.

(13) Hutton, A. C.; Kantsler, A. J.; Cook, A. C.; McKirdy, D. M. ORGANIC MATTER IN OIL SHALES. *APPEA J.* **1980**, *20* (1), 44–67. https://doi.org/10.1071/aj79005.

(14) Ross, D. J. K.; Marc Bustin, R. The Importance of Shale Composition and Pore Structure upon Gas Storage Potential of Shale Gas Reservoirs. *Mar. Pet. Geol.* **2009**, *26* (6), 916–927. https://doi.org/10.1016/j.marpetgeo.2008.06.004.

(15) Loucks, R. G.; Reed, R. M.; Ruppel, S. C.; Hammes, U. Spectrum of Pore Types and Networks in Mudrocks and a Descriptive Classification for Matrix-Related Mudrock PoresSpectrum of Pore Types and Networks In Mudrocks. *AAPG Bull.* **2012**, *96* (6), 1071–1098. https://doi.org/10.1306/08171111061.

(16) Clarkson, C. R.; Solano, N.; Bustin, R. M.; Bustin, A. M. M.; Chalmers, G. R. L.; He, L.; Melnichenko, Y. B.; Radliński, A. P.; Blach, T. P. Pore Structure Characterization of North American Shale Gas Reservoirs Using USANS/SANS, Gas Adsorption, and Mercury Intrusion. *Fuel* **2013**, *103*, 606–616. https://doi.org/10.1016/j.fuel.2012.06.119.

(17) Passey, Q. R.; Bohacs, K.; Esch, W. L.; Klimentidis, R.; Sinha, S. From Oil-Prone Source Rock to Gas-Producing Shale Reservoir - Geologic and Petrophysical Characterization of Unconventional Shale Gas Reservoirs; Society of Petroleum Engineers, 2010. https://doi.org/10.2118/131350-MS.

(18) Vernik, L.; Milovac, J. Rock Physics of Organic Shales. *Lead. Edge* **2011**, *30* (3), 318–323. https://doi.org/10.1190/1.3567263.

(19) Milliken, K. L.; Rudnicki, M.; Awwiller, D. N.; Zhang, T. Organic Matter–Hosted Pore System, Marcellus Formation (Devonian), PennsylvaniaGeohorizon. *AAPG Bull.* **2013**, *97* (2), 177–200. https://doi.org/10.1306/07231212048.

(20) Shabro, V.; Torres-Verdin, C.; Javadpour, F. Numerical Simulation of Shale-Gas Production: From Pore-Scale Modeling of Slip-Flow, Knudsen Diffusion, and Langmuir Desorption to Reservoir Modeling of Compressible Fluid; Society of Petroleum Engineers, 2011. https://doi.org/10.2118/144355-MS.

(21) Wu, K.; Li, X.; Wang, C.; Yu, W.; Chen, Z. Model for Surface Diffusion of Adsorbed Gas in Nanopores of Shale Gas Reservoirs. *Ind. Eng. Chem. Res.* **2015**, *54* (12), 3225–3236. https://doi.org/10.1021/ie504030v.

(22) Zaera, F. Probing Liquid/Solid Interfaces at the Molecular Level. *Chem. Rev.* **2012**, *112* (5), 2920–2986. https://doi.org/10.1021/cr2002068.

(23) *Surface Analysis Methods in Materials Science*; O'Connor, J., Sexton, B., Smart, R., Eds.; Springer Series in Surface Sciences; Springer-Verlag: Berlin Heidelberg, 1992.

(24) Mineralogical Society of America - Mineral-Water Interface Geochemistry http://www.minsocam.org/msa/rim/rim23.html (accessed Mar 13, 2019).

(25) Milner, M.; McLin, R.; Petriello, J. Imaging Texture and Porosity in Mudstones and Shales: Comparison of Secondary and Ion-Milled Backscatter SEM Methods; Society of Petroleum Engineers, 2010. https://doi.org/10.2118/138975-MS.

(26) Curtis, M. E.; Ambrose, R. J.; Sondergeld, C. H.; Rai, C. S. Transmission and Scanning Electron Microscopy Investigation of Pore Connectivity of Gas Shales on the Nanoscale; Society of Petroleum Engineers, 2011. https://doi.org/10.2118/144391-MS.

(27) Bernard, S.; Horsfield, B.; Schulz, H.-M.; Wirth, R.; Schreiber, A.; Sherwood, N. Geochemical Evolution of Organic-Rich Shales with Increasing Maturity: A STXM and TEM Study of the Posidonia Shale (Lower Toarcian, Northern Germany). *Mar. Pet. Geol.* **2012**, *31* (1), 70–89. https://doi.org/10.1016/j.marpetgeo.2011.05.010.

(28) Javadpour, F.; Moravvej Farshi, M.; Amrein, M. Atomic-Force Microscopy: A New Tool for Gas-Shale Characterization. *J. Can. Pet. Technol.* **2012**, *51* (04), 236–243. https://doi.org/10.2118/161015-PA.

(29) Bhargava, S.; Awaja, F.; Subasinghe, N. D. Characterisation of Some Australian Oil Shale Using Thermal, X-Ray and IR Techniques. *Fuel* **2005**, *84* (6), 707–715. https://doi.org/10.1016/j.fuel.2004.11.013.

(30) Elgmati, M. M.; Zhang, H.; Bai, B.; Flori, R. E.; Qu, Q. Submicron-Pore Characterization of Shale Gas Plays; Society of Petroleum Engineers, 2011. https://doi.org/10.2118/144050-MS.

(31) Tiwari, P.; Deo, M.; Lin, C. L.; Miller, J. D. Characterization of Oil Shale Pore Structure before and after Pyrolysis by Using X-Ray Micro CT. *Fuel* **2013**, *107*, 547–554. https://doi.org/10.1016/j.fuel.2013.01.006.

(32) Duliu, O. G. Computer Axial Tomography in Geosciences: An Overview. *Earth-Sci. Rev.* **1999**, *48* (4), 265–281. https://doi.org/10.1016/S0012-8252(99)00056-2.

(33) Kadayam Viswanathan, R. K.; Cao Minh, C.; Zielinski, L.; Vissapragada, B.; Akkurt, R.; Song, Y.-Q.; Liu, C.; Jones, S.; Blair, E. Characterization of Gas Dynamics in Kerogen Nanopores by NMR; Society of Petroleum Engineers, 2011. https://doi.org/10.2118/147198-MS.

(34) Korb, J.-P.; Nicot, B.; Louis-Joseph, A.; Bubici, S.; Ferrante, G. Dynamics and Wettability of Oil and Water in Oil Shales. *J. Phys. Chem. C* **2014**, *118* (40), 23212–23218. https://doi.org/10.1021/jp508659e.

(35) Cygan, R. T. Molecular Modeling in Mineralogy and Geochemistry. *Rev. Mineral. Geochem.* **2001**, *42* (1), 1–35. https://doi.org/10.2138/rmg.2001.42.1.

(36) Allen, M.; Tildesley, D. *Computer Simulation of Liquids*, Second Edition.; Oxford University Press: Oxford, New York, 2017.

(37) Frenkel, D.; Smit, B. *Understanding Molecular Simulation: From Algorithms to Applications*, Second Edition.; Academic Press: San Diego, 2002.

(38) Collell, J.; Galliero, G.; Gouth, F.; Montel, F.; Pujol, M.; Ungerer, P.; Yiannourakou, M. Molecular Simulation and Modelisation of Methane/Ethane Mixtures Adsorption onto a Microporous Molecular Model of Kerogen under Typical Reservoir Conditions. *Microporous Mesoporous Mater.* **2014**, *197*, 194–203. https://doi.org/10.1016/j.micromeso.2014.06.016.

(39) Collell, J.; Galliero, G.; Vermorel, R.; Ungerer, P.; Yiannourakou, M.; Montel, F.; Pujol, M. Transport of Multicomponent Hydrocarbon Mixtures in Shale Organic Matter by Molecular Simulations. *J. Phys. Chem. C* **2015**, *119* (39), 22587–22595. https://doi.org/10.1021/acs.jpcc.5b07242.

(40) Collell, J.; Ungerer, P.; Galliero, G.; Yiannourakou, M.; Montel, F.; Pujol, M. Molecular Simulation of Bulk Organic Matter in Type II Shales in the Middle of the Oil Formation Window. *Energy Fuels* **2014**, *28* (12), 7457–7466. https://doi.org/10.1021/ef5021632.

(41) Sui, H.; Yao, J. Effect of Surface Chemistry for CH4/CO2 Adsorption in Kerogen: A Molecular Simulation Study. *J. Nat. Gas Sci. Eng.* **2016**, *31*, 738–746. https://doi.org/10.1016/j.jngse.2016.03.097.

(42) Yiannourakou, M.; Ungerer, P.; Leblanc, B.; Rozanska, X.; Saxe, P.; Vidal-Gilbert, S.; Gouth, F.; Montel, F. Molecular Simulation of Adsorption in Microporous Materials. *Oil Gas Sci. Technol. – Rev. D'IFP Energ. Nouv.* **2013**, *68* (6), 977–994. https://doi.org/10.2516/ogst/2013134.

(43) Lee, T.; Bocquet, L.; Coasne, B. Activated Desorption at Heterogeneous Interfaces and Long-Time Kinetics of Hydrocarbon Recovery from Nanoporous Media. *Nat. Commun.* **2016**, *7*, 11890. https://doi.org/10.1038/ncomms11890.

(44) Wang, S.; Javadpour, F.; Feng, Q. Molecular Dynamics Simulations of Oil Transport through Inorganic Nanopores in Shale. *Fuel* **2016**, *171*, 74–86. https://doi.org/10.1016/j.fuel.2015.12.071.

(45) Wang, S.; Feng, Q.; Javadpour, F.; Yang, Y.-B. Breakdown of Fast Mass Transport of Methane through Calcite Nanopores. *J. Phys. Chem. C* **2016**, *120* (26), 14260–14269. https://doi.org/10.1021/acs.jpcc.6b05511.

(46) Zheng, H.; Du, Y.; Xue, Q.; Zhu, L.; Li, X.; Lu, S.; Jin, Y. Surface Effect on Oil Transportation in Nanochannel: A Molecular Dynamics Study. *Nanoscale Res. Lett.* **2017**, *12* (1), 413. https://doi.org/10.1186/s11671-017-2161-2.

(47) Liu, Q.; Yuan, S.; Yan, H.; Zhao, X. Mechanism of Oil Detachment from a Silica Surface in Aqueous Surfactant Solutions: Molecular Dynamics Simulations. *J. Phys. Chem. B* **2012**, *116* (9), 2867–2875. https://doi.org/10.1021/jp2118482.

(48) Ambrose, R. J.; Hartman, R. C.; Diaz-Campos, M.; Akkutlu, I. Y.; Sondergeld, C. H. Shale Gas-in-Place Calculations Part I: New Pore-Scale Considerations. *SPE J.* **2012**, *17* (01), 219–229. https://doi.org/10.2118/131772-PA.

(49) Underwood, T.; Erastova, V.; Cubillas, P.; Greenwell, H. C. Molecular Dynamic Simulations of Montmorillonite–Organic Interactions under Varying Salinity: An Insight into Enhanced Oil Recovery. *J. Phys. Chem. C* **2015**, *119* (13), 7282–7294. https://doi.org/10.1021/acs.jpcc.5b00555.

(50) Kästner, J. Umbrella Sampling. *Wiley Interdiscip. Rev. Comput. Mol. Sci.* **2011**, *1* (6), 932–942. https://doi.org/10.1002/wcms.66.

(51) Hughey, C. A.; Rodgers, R. P.; Marshall, A. G.; Qian, K.; Robbins, W. K. Identification of Acidic NSO Compounds in Crude Oils of Different Geochemical Origins by Negative Ion Electrospray Fourier Transform Ion Cyclotron Resonance Mass Spectrometry. *Org. Geochem.* **2002**, *33* (7), 743–759. https://doi.org/10.1016/S0146-6380(02)00038-4.

(52) Hyne, N. J. *Nontechnical Guide to Petroleum Geology, Exploration, Drilling, and Production*; PennWell Corporation: Tulsa, Okla., 2012.

(53) Buckley, J. S.; Liu, Y.; Monsterleet, S. Mechanisms of Wetting Alteration by Crude Oils. *SPE J.* **1998**, *3* (01), 54–61. https://doi.org/10.2118/37230-PA.

(54) Sayyouh, M. H.; Hemeida, A. M.; Al-Blehed, M. S.; Desouky, S. M. Role of Polar Compounds in Crude Oils on Rock Wettability. *J. Pet. Sci. Eng.* **1991**, *6* (3), 225–233. https://doi.org/10.1016/0920-4105(91)90015-F.

(55) Speight, J. G. The Chemical and Physical Structure of Petroleum: Effects on Recovery Operations. *J. Pet. Sci. Eng.* **1999**, *22* (1), 3–15. https://doi.org/10.1016/S0920-4105(98)00051-5.

(56) Composition, Classification, and Properties of Petroleum. In *Chemistry of Fossil Fuels and Biofuels*; Schobert, H., Ed.; Cambridge Series in Chemical Engineering; Cambridge University Press: Cambridge, 2013; pp 174–191. https://doi.org/10.1017/CBO9780511844188.012.

(57) Mango, F. D. The Light Hydrocarbons in Petroleum: A Critical Review. *Org. Geochem.* **1997**, *26* (7), 417–440. https://doi.org/10.1016/S0146-6380(97)00031-4.

(58) Yanik, J.; Yüksel, M.; Sağlam, M.; Olukçu, N.; Bartle, K.; Frere, B. Characterization of the Oil Fractions of Shale Oil Obtained by Pyrolysis and Supercritical Water Extraction. *Fuel* **1995**, *74* (1), 46–50. https://doi.org/10.1016/0016-2361(94)P4329-Z.

(59) Kvashnin, D. G.; Antipina, L. Y.; Sorokin, P. B.; Tenne, R.; Golberg, D. Theoretical Aspects of WS2 Nanotube Chemical Unzipping. *Nanoscale* **2014**, *6* (14), 8400–8404. https://doi.org/10.1039/C4NR00437J.

(60) Berendsen, H. J. C.; Postma, J. P. M.; van Gunsteren, W. F.; Hermans, J. Interaction Models for Water in Relation to Protein Hydration. In *Intermolecular Forces: Proceedings of the Fourteenth Jerusalem Symposium on Quantum Chemistry and Biochemistry Held in Jerusalem, Israel, April 13–16, 1981*; Pullman, B., Ed.; The Jerusalem Symposia on Quantum Chemistry and Biochemistry; Springer Netherlands: Dordrecht, 1981; pp 331–342. https://doi.org/10.1007/978-94-015-7658-1_21.

(61) Kerisit, S.; Parker, S. C. Free Energy of Adsorption of Water and Metal Ions on the {10$\bar{1}$4} Calcite Surface. *J. Am. Chem. Soc.* **2004**, *126* (32), 10152–10161. https://doi.org/10.1021/ja0487776.

(62) Curtis, J. B. Fractured Shale-Gas Systems. *AAPG Bull.* **2002**, *86* (11), 1921–1938. https://doi.org/10.1306/61EEDDBE-173E-11D7-8645000102C1865D.

(63) Jarvie, D. M.; Hill, R. J.; Ruble, T. E.; Pollastro, R. M. Unconventional Shale-Gas Systems: The Mississippian Barnett Shale of North-Central Texas as One Model for Thermogenic Shale-Gas Assessment. *AAPG Bull.* **2007**, *91* (4), 475–499. https://doi.org/10.1306/12190606068.

(64) Vandenbroucke, M.; Largeau, C. Kerogen Origin, Evolution and Structure. *Org. Geochem.* **2007**, *38* (5), 719–833. https://doi.org/10.1016/j.orggeochem.2007.01.001.

(65) Hu, Y.; Devegowda, D.; Striolo, A.; Phan, A.; Ho, T. A.; Civan, F.; Sigal, R. F. Microscopic Dynamics of Water and Hydrocarbon in Shale-Kerogen Pores of Potentially Mixed Wettability. *SPE J.* **2014**, *20* (01), 112–124. https://doi.org/10.2118/167234-PA.

(66) Firouzi, M.; Rupp, E. C.; Liu, C. W.; Wilcox, J. Molecular Simulation and Experimental Characterization of the Nanoporous Structures of Coal and Gas Shale. *Int. J. Coal Geol.* **2014**, *121*, 123–128. https://doi.org/10.1016/j.coal.2013.11.003.

(67) Falk, K.; Pellenq, R.; Ulm, F. J.; Coasne, B. Effect of Chain Length and Pore Accessibility on Alkane Adsorption in Kerogen. *Energy Fuels* **2015**, *29* (12), 7889–7896. https://doi.org/10.1021/acs.energyfuels.5b02015.

(68) Ambrose, R. J.; Hartman, R. C.; Diaz Campos, M.; Akkutlu, I. Y.; Sondergeld, C. New Pore-Scale Considerations for Shale Gas in Place Calculations; Society of Petroleum Engineers, 2010. https://doi.org/10.2118/131772-MS.

(69) Orendt, A. M.; Pimienta, I. S. O.; Badu, S. R.; Solum, M. S.; Pugmire, R. J.; Facelli, J. C.; Locke, D. R.; Chapman, K. W.; Chupas, P. J.; Winans, R. E. Three-Dimensional Structure of the Siskin Green River Oil Shale Kerogen Model: A Comparison between Calculated and Observed Properties. *Energy Fuels* **2013**, *27* (2), 702–710. https://doi.org/10.1021/ef3017046.

(70) Bousige, C.; Ghimbeu, C. M.; Vix-Guterl, C.; Pomerantz, A. E.; Suleimenova, A.; Vaughan, G.; Garbarino, G.; Feygenson, M.; Wildgruber, C.; Ulm, F.-J.; et al. Realistic Molecular Model of Kerogen's Nanostructure. *Nat. Mater.* **2016**, *15* (5), 576–582. https://doi.org/10.1038/nmat4541.

(71) Pei, Q.-X.; Zhang, Y.-W.; Shenoy, V. B. Mechanical Properties of Methyl Functionalized Graphene: A Molecular Dynamics Study. *Nanotechnology* **2010**, *21* (11), 115709. https://doi.org/10.1088/0957-4484/21/11/115709.

(72) Lee, S. S.; Heberling, F.; Sturchio, N. C.; Eng, P. J.; Fenter, P. Surface Charge of the Calcite (104) Terrace Measured by Rb+ Adsorption in Aqueous Solutions Using Resonant Anomalous X-Ray Reflectivity. *J. Phys. Chem. C* **2016**, *120* (28), 15216–15223. https://doi.org/10.1021/acs.jpcc.6b04364.

(73) Wolthers, M.; Tommaso, D. D.; Du, Z.; Leeuw, N. H. de. Calcite Surface Structure and Reactivity: Molecular Dynamics Simulations and Macroscopic Surface Modelling of the Calcite –Water Interface. *Phys. Chem. Chem. Phys.* **2012**, *14* (43), 15145–15157. https://doi.org/10.1039/C2CP42290E.

(74) Alipour Tabrizy, V.; Denoyel, R.; Hamouda, A. A. Characterization of Wettability Alteration of Calcite, Quartz and Kaolinite: Surface Energy Analysis. *Colloids Surf. Physicochem. Eng. Asp.* **2011**, *384* (1), 98–108. https://doi.org/10.1016/j.colsurfa.2011.03.021.

(75) Sposito, G.; Skipper, N. T.; Sutton, R.; Park, S.; Soper, A. K.; Greathouse, J. A. Surface Geochemistry of the Clay Minerals. *Proc. Natl. Acad. Sci.* **1999**, *96* (7), 3358–3364. https://doi.org/10.1073/pnas.96.7.3358.

(76) Robertson, M. J.; Tirado-Rives, J.; Jorgensen, W. L. Improved Peptide and Protein Torsional Energetics with the OPLS-AA Force Field. *J. Chem. Theory Comput.* **2015**, *11* (7), 3499–3509. https://doi.org/10.1021/acs.jctc.5b00356.

(77) Raiteri, P.; Gale, J. D.; Quigley, D.; Rodger, P. M. Derivation of an Accurate Force-Field for Simulating the Growth of Calcium Carbonate from Aqueous Solution: A New Model for the Calcite−Water Interface. *J. Phys. Chem. C* **2010**, *114* (13), 5997–6010. https://doi.org/10.1021/jp910977a.

(78) Geissbühler, P.; Fenter, P.; DiMasi, E.; Srajer, G.; Sorensen, L. B.; Sturchio, N. C. Three-Dimensional Structure of the Calcite–Water Interface by Surface X-Ray Scattering. *Surf. Sci.* **2004**, *573* (2), 191–203. https://doi.org/10.1016/j.susc.2004.09.036.

(79) Wolf, G.; Lerchner, J.; Schmidt, H.; Gamsjäger, H.; Königsberger, E.; Schmidt, P. Thermodynamics of CaCO3 Phase Transitions. *J. Therm. Anal. Calorim.* **1996**, *46* (2), 353–359. https://doi.org/10.1007/BF02135013.

(80) Wolf, G.; Königsberger, E.; Schmidt, H. G.; Königsberger, L.-C.; Gamsjäger, H. Thermodynamic Aspects of the Vaterite-Calcite Phase Transition. *J. Therm. Anal. Calorim.* **2000**, *60* (2), 463–472. https://doi.org/10.1023/A:1010114131577.

(81) Kumar, S.; Rosenberg, J. M.; Bouzida, D.; Swendsen, R. H.; Kollman, P. A. THE Weighted Histogram Analysis Method for Free-Energy Calculations on Biomolecules. I. The Method. *J. Comput. Chem.* **1992**, *13* (8), 1011–1021. https://doi.org/10.1002/jcc.540130812.

(82) Roux, B. The Calculation of the Potential of Mean Force Using Computer Simulations. *Comput. Phys. Commun.* **1995**, *91* (1), 275–282. https://doi.org/10.1016/0010-4655(95)00053-I.

(83) Hakim, S. S.; Olsson, M. H. M.; Sørensen, H. O.; Bovet, N.; Bohr, J.; Feidenhans'l, R.; Stipp, S. L. S. Interactions of the Calcite {10.4} Surface with Organic Compounds: Structure and Behaviour at Mineral – Organic Interfaces. *Sci. Rep.* **2017**, *7* (1), 7592. https://doi.org/10.1038/s41598-017-06977-4.

(84) Ross, D. J. K.; Bustin, R. M. Shale Gas Potential of the Lower Jurassic Gordondale Member, Northeastern British Columbia, Canada. *Bull. Can. Pet. Geol.* **2007**, *55* (1), 51–75. https://doi.org/10.2113/gscpgbull.55.1.51.

(85) Loucks, R. G.; Reed, R. M.; Ruppel, S. C.; Jarvie, D. M. Morphology, Genesis, and Distribution of Nanometer-Scale Pores in Siliceous Mudstones of the Mississippian Barnett Shale. *J. Sediment. Res.* **2009**, *79* (12), 848–861. https://doi.org/10.2110/jsr.2009.092.

(86) Madsen, L.; Grahl-Madsen, L.; Grøn, C.; Lind, I.; Engell, J. Adsorption of Polar Aromatic Hydrocarbons on Synthetic Calcite. *Org. Geochem.* **1996**, *24* (12), 1151–1155. https://doi.org/10.1016/S0146-6380(96)00096-4.

(87) Crocker, M. E.; Marchin, L. M. Wettability and Adsorption Characteristics of Crude-Oil Asphaltene and Polar Fractions. *J. Pet. Technol.* **1988**, *40* (04), 470–474. https://doi.org/10.2118/14885-PA.

(88) He, L.; Lin, F.; Li, X.; Sui, H.; Xu, Z. Interfacial Sciences in Unconventional Petroleum Production: From Fundamentals to Applications. *Chem. Soc. Rev.* **2015**, *44* (15), 5446–5494. https://doi.org/10.1039/C5CS00102A.

(89) Morrow, N. R. Wettability and Its Effect on Oil Recovery. *J. Pet. Technol.* **1990**, *42* (12), 1,476-1,484. https://doi.org/10.2118/21621-PA.

(90) García Carmona, J.; Gómez Morales, J.; Rodríguez Clemente, R. Rhombohedral–Scalenohedral Calcite Transition Produced by Adjusting the Solution Electrical Conductivity in the System Ca(OH)2–CO2–H2O. *J. Colloid Interface Sci.* **2003**, *261* (2), 434–440. https://doi.org/10.1016/S0021-9797(03)00149-8.

(91) Shen, J.-W.; Li, C.; van der Vegt, N. F. A.; Peter, C. Understanding the Control of Mineralization by Polyelectrolyte Additives: Simulation of Preferential Binding to Calcite Surfaces. *J. Phys. Chem. C* **2013**, *117* (13), 6904–6913. https://doi.org/10.1021/jp402341w.

605

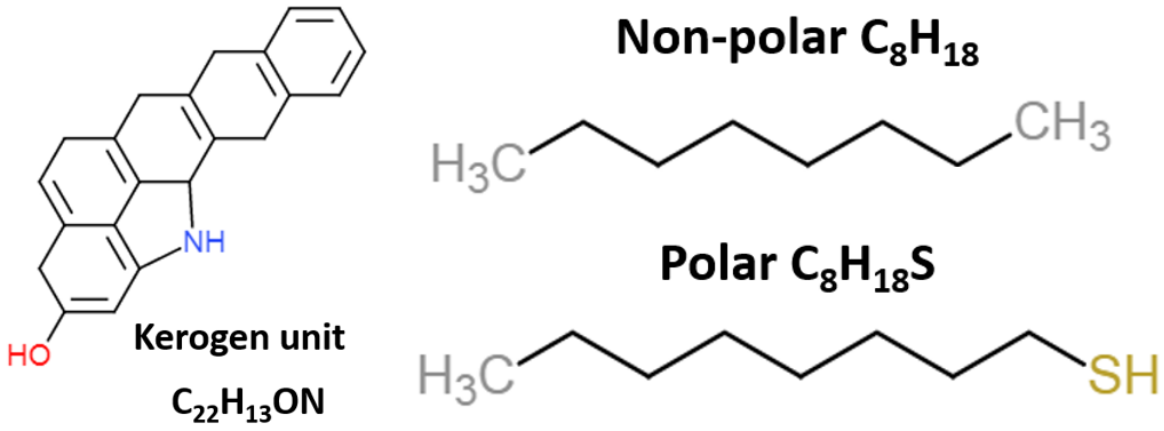

Figure 1. Molecular structure of type II kerogen fragment (left), non-polar oil n-octane (right top), and polar oil 1-octanethiol (right bottom).

606

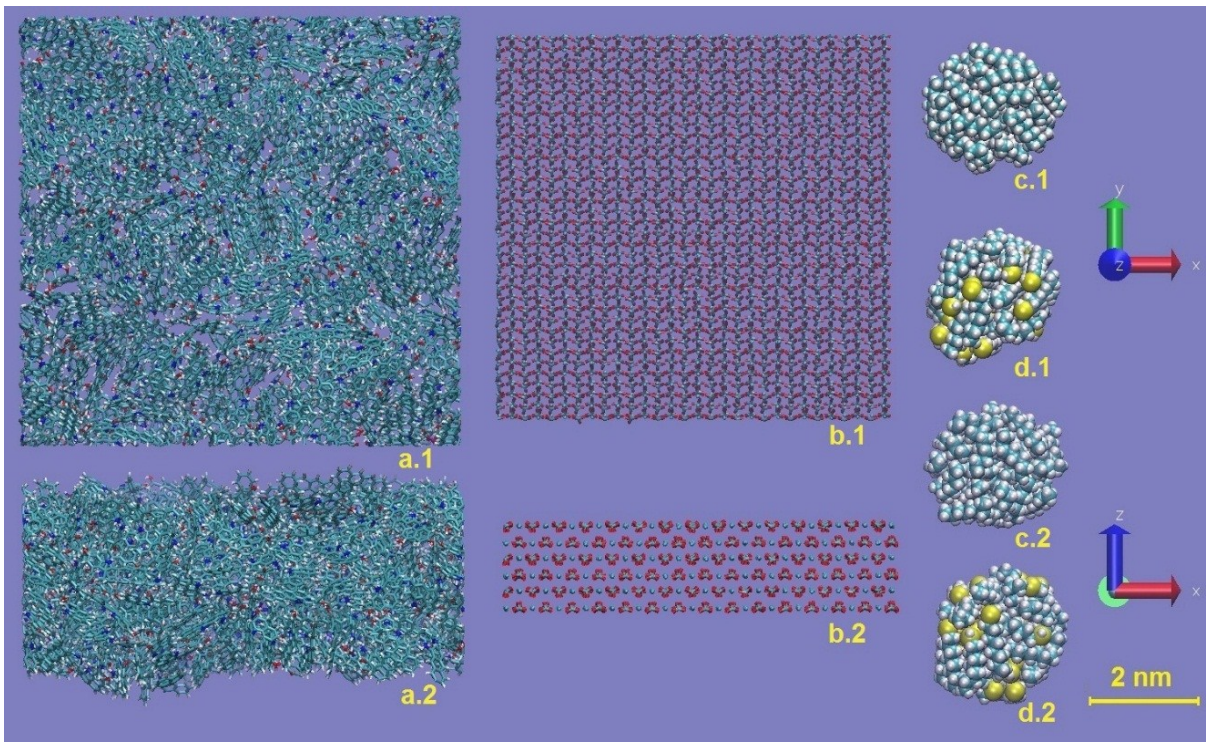

Figure 2. Kerogen slab (a), calcite {104} slab (b), 30-molecule non-polar oil cluster (c), and 30-molecule polar oil cluster (d). "x.1" and "x.2" denote different orientations.

607

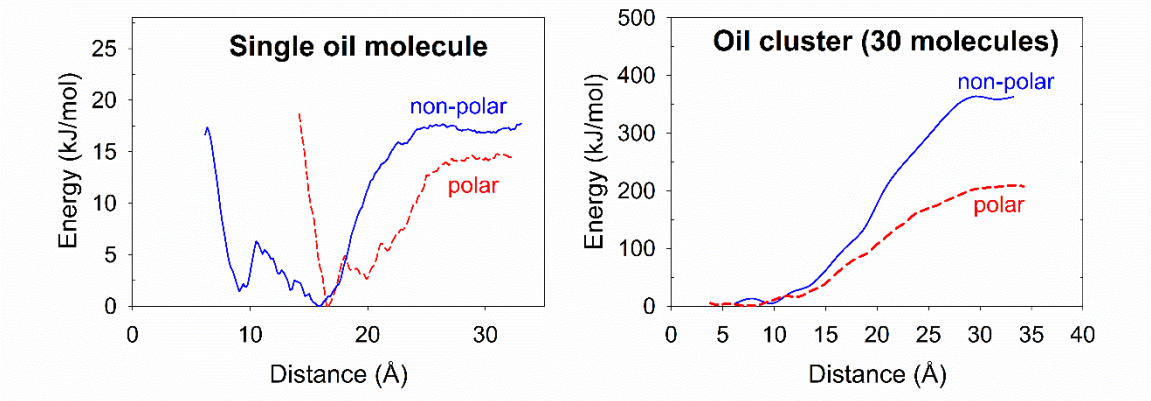

Figure 3. Free energy surfaces of single molecule of polar or non-polar oil on kerogen surface with water (left); Free energy surfaces of oil drop of 30 polar or non-polar oil molecules on kerogen surface with water (right).

608

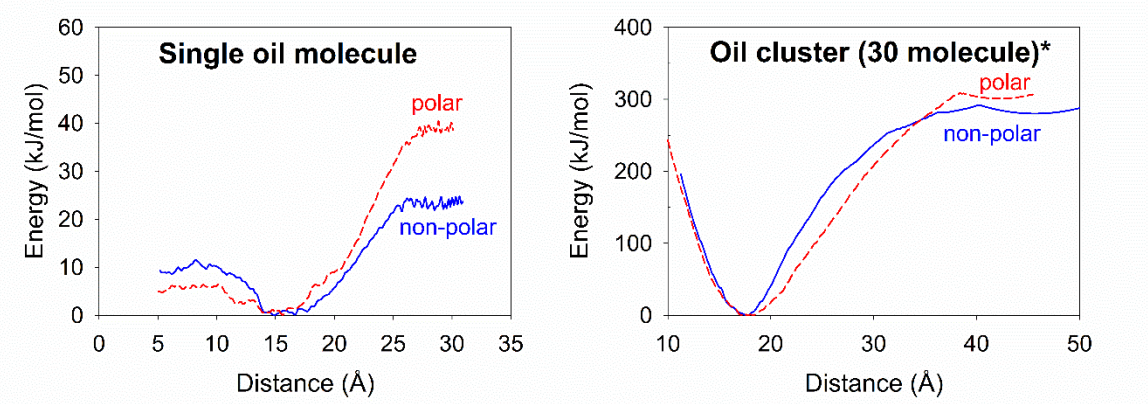

Figure 4. Free energy surfaces of single molecule of polar and non-polar oil on kerogen surface without water (left); free energy surfaces of oil drop of 30 polar or non-polar oil molecules on kerogen surface without water (right). *indicates the simulations were prepared 200K due to the technical issues as described in the discussion.

609

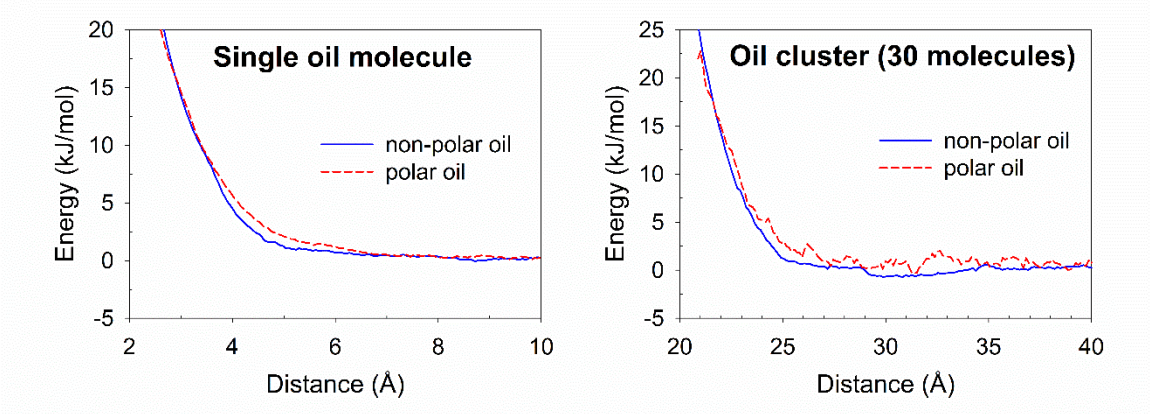

Figure 5. Free energy surfaces of single molecule and 30-molecule cluster of polar or non-polar oil on calcite surface in the presence of water.

610

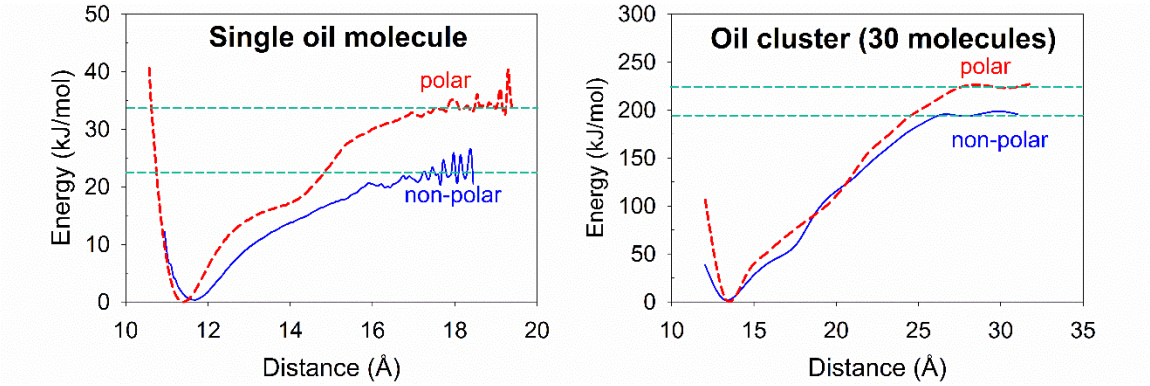

Figure 6. Free energy surfaces of single molecule of polar or non-polar oil on calcite surface without water (left); free energy surfaces of oil drop of polar or non-polar oil on calcite surface without water (right).

Table 1. Desorption energy of single molecule oil droplet and 30-molecule oil drop on calcite and kerogen surface under 300 K. The ( ) denotes the errors propagated from the output data of WHAM.

Desorption energy (kJ/mol)		Kerogen with water	Kerogen	Calcite with water	Calcite
Non-polar	Single molecule	17.0 (2.0)	23.3 (3.5)	0	18.0 (5.5)
	Cluster	372 (13.8)	438 (13. 5)	0	198 (42)
Polar oil	Single molecule	16.5 (3.3)	39.5 (9.5)	0	33.6 (3.9)
	Cluster	210 (11.4)	438 (13.5)	0	222 (36)
Desorption energy per molecule (kJ/mol)		Kerogen with water	Kerogen	Calcite with water	Calcite
Non-polar	Single molecule	17.0 (2.0)	23.3 (3.5)	0	18.0 (5.5)
	Cluster	12.4 (0.46)	14.6 (0.45)	0	6.6 (1.4)
Polar oil	Single molecule	16.5 (3.3)	39.5 (9.5)	0	33.6 (3.9)
	Cluster	7.0 (0.38)	14.6 (0.45)	0	7.4 (1.2)

612 **Supplement Information**
613

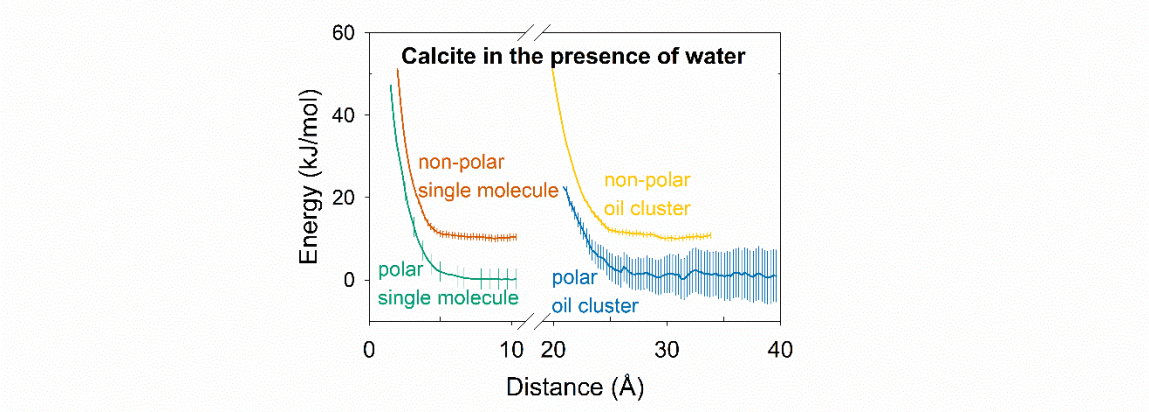

614

615 Fig S1. Free energy surfaces of oil drop of polar or non-polar oil on calcite surface with water. The
616 density of displayed data is reduced for visual clarity.

617

618

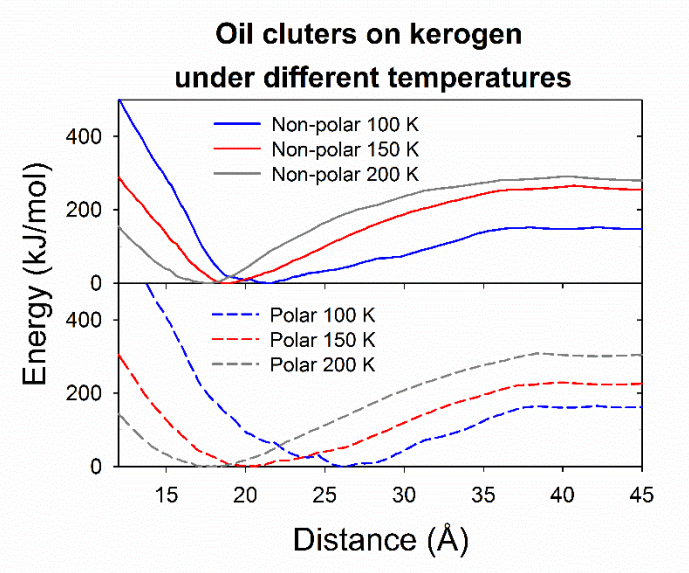

619

620 Fig S2. Free energy surfaces of 30-molecule oil drops interacting with kerogen surface under different
621 temperatures. According to the data point pattern on this chart, the correlation between desorption energy
622 and temperature can be formulated using the same equation below for both polar and non-polar oil. The
623 error bars are smaller than the symbol size.

624

625 SI Table 1. Desorption energies of oil drops on kerogen surface under different temperatures.

Desorption energy in kJ/mol [error]		
Temperature	Non-polar	Polar
100 K	150.5 [2.5]	163 [3]
150 K	260 [5.5]	226 [3]
200 K	285 [5.5]	304 [5]

626

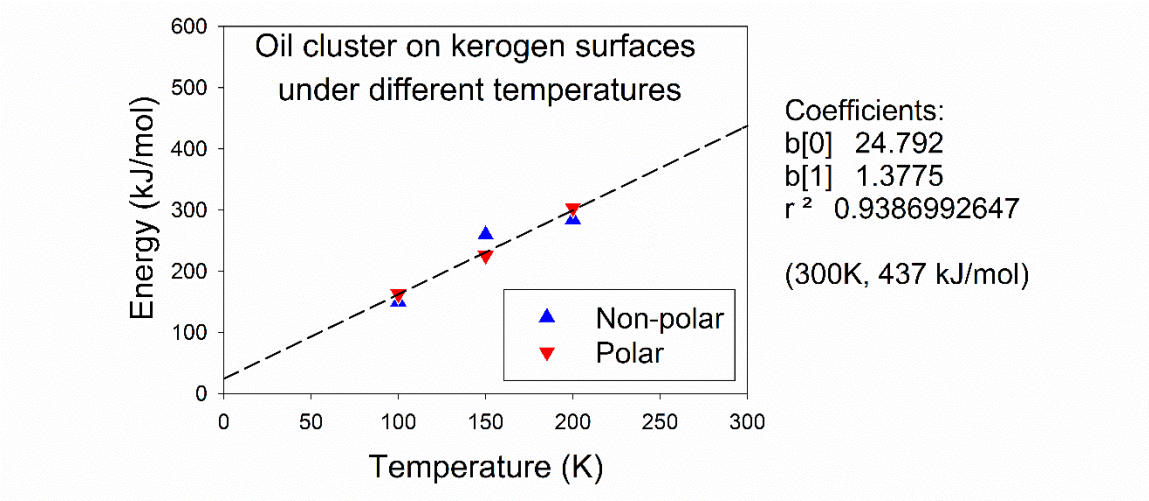

Fig S3. Desorption energies of 30-molecule oil drops on kerogen surfaces under different temperatures.

The non-polar and polar oil drops exhibit linear relationship between temperature and desorption energy (with a R-squared value of 0.9387). The non-polar and polar oil drops follow the same correlation between desorption energy (E_d in kJ/mol) and temperature (T in K):

$$E_d = 1.38 \cdot T + 24.8$$

The energy required for oil drop desorption from kerogen surface increases when the system temperature rises. As shown in Fig 9, a close examination on the interface of oil and surface reveals that molecules of oil drop are strongly attached to the kerogen surface. The same correlation of energy and temperature suggested that the intermolecular bonding between kerogen and oil are so strong that the effect of oil polarity is negligible during such interactions.